Sociedade Portuguesa de Reologia

Livro de Actas
Proceedings

2º Encontro Nacional da SPR

7 e 8 de Abril de 2000

Faculdade de Engenharia
da Universidade do Porto

PORTO

THE FLOW OF UCM FLUIDS PAST A CYLINDER

M.A. Alves[a], F. T. Pinho[b] and P. J. Oliveira[c]

[a]Departamento de Engenharia Química, Centro de Estudos de Fenómenos de Transporte, Faculdade de Engenharia Universidade do Porto, Rua dos Bragas, 4050-123 Porto, Portugal

[b]Centro de Estudos de Fenómenos de Transporte, Departamento de Engenharia Mecânica, Faculdade de Engenharia, Universidade do Porto, Rua dos Bragas, 4050-123 Porto, Portugal

[c]Departamento de Engenharia Electromecânica, Universidade da Beira Interior Rua Marquês D'Ávila e Bolama, 6200 Covilhã, Portugal

Resumo

O método de cálculo de escoamentos viscoelásticos desenvolvido por Oliveira et al [1], e baseado na formulação de volumes finitos, foi modificado para combinar esquemas de interpolação de segunda ordem com um critério de limitação, resultando daí uma maior precisão e estabilidade. O programa de simulação funciona com malhas 3D não-ortogonais e semi-estruturadas (em bloco), com arranjo colocado das variáveis e endereçamento indirecto para um mapeamento de geometrias complexas mais eficiente. O programa foi aqui utilizado para prever o escoamento sem inércia de fluidos convectivos superiores de Maxwell (UCM) em torno de um cilindro bidimensional num canal, um conhecido escoamento de calibração. Os resultados das simulações são considerados mais precisos que os de Fan et al [2], obtidos por simulação numérica com o método mais dispendioso dos elementos finitos.

Abstract

The general colocated FVM procedure for viscoelastic flows developed by Oliveira et al [1] has been modified to combine a second-order interpolation schemes with a boundedness criterion for improved accuracy and stability. The code relies on block-structured, colocated, nonorthogonal 3D grids with indirect addressing for easy mapping of complex geometries, and it was used here to predict the inertialess plane flow around a cylinder in a duct, a well-known benchmark case. Under investigation was the upper convected Maxwell (UCM) fluid and the results are judged to be more accurate than data of Fan et al [2], which was obtained with the more expensive finite-element method.

KEYWORDS: finite-volume method, high-resolution scheme, cylinder flow, UCM

1. Introduction

The increasing use of computational tools to design industrial equipment requires the ability to predict well the flow of viscoelastic fluids. The two-dimensional flow around a cylinder in a channel is relevant for industrial applications, and because of the difficulties associated with the development of thin stress layers on the cylinder surface and along the cylinder wake it has been used as a benchmark flow [3]. There has been an enormous effort to develop adequate codes and numerical procedures for the prediction of viscoelastic flows based on the finite-element method (FEM)[2,4-5], and recently these have been tested against this benchmark problem.

Finite-volume methods (FVM) are serious alternatives to FEM codes for viscoelastic computations as they can be very advantageous in computing resources [6], but far less effort has been dedicated to the FVM technique than to finite elements. FVM procedures for viscoelastic flows have been presented by Phan-Thien and co-workers for orthogonal staggered meshes [7] and a form of unstructured meshes [6,8], and by Oliveira et al [1,9-10] for semi-

structured meshes, for easy mapping of complex geometries. Further improvements require the use of second- or higher-order interpolation schemes for the convective terms of the constitutive equation, but then stability must be enforced via appropriate boundedness criteria [10]. This combination leads to the so-called high-resolution schemes and in this paper one such method is used to predict the benchmark cylinder flow of upper convected Maxwell (UCM) fluids with similar or better results than other advanced FEM methods [2].

Section 2 presents the governing equations, the numerical method is briefly described in Section 3. and the results of the simulations are presented and discussed in Section 4.

2. Governing equations

The method solves the system of equations of conservation of mass and linear momentum, and the constitutive equation for an UCM fluid, which are written as follows:

$$\frac{\partial u_i}{\partial x_i} = 0 \tag{1}$$

$$\frac{\partial \rho u_i}{\partial t} + \frac{\partial \rho u_j u_i}{\partial x_j} - \frac{\partial}{\partial x_j}\left(\eta \frac{\partial u_i}{\partial x_j}\right) = -\frac{\partial p}{\partial x_i} + \rho g_i + \frac{\partial \tau_{ij}}{\partial x_j} - \frac{\partial}{\partial x_j}\left(\eta \frac{\partial u_i}{\partial x_j}\right) \tag{2}$$

$$\tau_{ij} + \lambda\left(\frac{\partial \tau_{ij}}{\partial t} + u_k \frac{\partial \tau_{ij}}{\partial x_k}\right) = \eta\left(\frac{\partial u_i}{\partial x_j} + \frac{\partial u_j}{\partial x_i} - \frac{2}{3}\frac{\partial u_k}{\partial x_k}\delta_{ij}\right) + \lambda\left(\tau_{jk}\frac{\partial u_i}{\partial x_k} + \tau_{ik}\frac{\partial u_j}{\partial x_k}\right) \tag{3}$$

where ρ is the density of the fluid, u_i is the Cartesian velocity component along x_i, p is the pressure, λ is the relaxation time, δ_{ij} is the Kronecker delta and η is the shear viscosity. In the solution algorithm, the terms on l.h.s. of Eqs. (2) and (3) are dealt with implicitly, while those on the r.h.s. go into the source term of the matrix equations that result from the discretization procedure.

3. Numerical Method

Equations (1)-(3) are transformed into a general nonorthogonal co-ordinate system for application of the FVM method to a colocated mesh arrangement, prior to integration over the set of control volumes (cells) and final discretisation. The dependent variables remain the Cartesian velocity and stress components and the pressure, all stored at the centre of the cells. To avoid stress-velocity decoupling, a special procedure explained in the previous works [1,9] is adopted for the calculation of the stress divergent term in the momentum equation. The novelty of this work is the high-resolution scheme used to interpolate the cell-face stresses originating in the convective terms of the constitutive equation, and only this issue will be addressed in detail below. Other details of the numerical method are given in [1,9,10].

3.1. Constitutive equation

The discretised form of the constitutive equation is casted in the usual form at a general cell P of volume V_P

$$a_{\mathrm{P}}\tau_{ij,\mathrm{P}} - \sum_{\mathrm{F}} a_{\mathrm{F}}\tau_{ij,\mathrm{F}} = S_{\tau_{ij}} + \frac{\lambda V_{\mathrm{P}}}{\delta t}\tau^{0}_{ij,\mathrm{P}} \tag{4}$$

where the coefficients a_{F} are composed only by convective contributions. In the present procedure, a high-resolution scheme is used together with the deferred correction approach of Rubin and Khosla [11]. Here, convective contributions based on the upwind differencing scheme (UDS) are added to both hands of Eq. (4). The convective contribution on the l.h.s. is handled implicitly and on the r.h.s. the difference between the higher-order high-resolution scheme and the upwind scheme is handled explicitly in the context of time advancement. The source term in Eq. (4) also incorporates the part of the Oldroyd derivative on the r.h.s. of Eq. (3) which is evaluated with central differencing.

3.2. High-resolution differencing scheme (HRS)

In the FVM procedure, upon integration of the convective terms of the constitutive equation and the application of Gauss' theorem one ends up with convective fluxes at cell faces and these need to be equated as a function of nodal values via appropriate interpolation schemes. The HRS adopted here was developed within the context of the normalised variable and space formulation (NVSF) of Darwish and Moukalled [13].

In the NVSF the convected stress component τ_{ij} and the general curvilinear co-ordinate ξ are normalised as

$$\tilde{\tau}_{ij} = \frac{\tau_{ij} - \tau_{ij,\mathrm{U}}}{\tau_{ij,\mathrm{D}} - \tau_{ij,\mathrm{U}}} \tag{5}$$

$$\tilde{\xi} = \frac{\xi - \xi_{\mathrm{U}}}{\xi_{\mathrm{D}} - \xi_{\mathrm{U}}} \tag{6}$$

where the subscripts U and D refer to the upstream and downstream cells to cell P, which is the cell immediately upstream of cell face f under consideration.

To satisfy the convection boundedness criterion (CBC) of Gaskell and Lau [14] the functional relationship of an interpolation scheme applied to a cell-face f, $\tilde{\tau}_{ij,f} = \vartheta\left(\tilde{\tau}_{ij,\mathrm{P}}\right)$, must be continuous and bounded from below by $\tilde{\tau}_{ij,f} = \tilde{\tau}_{ij,\mathrm{P}}$ and from above by 1 in the range $0 < \tilde{\tau}_{ij,\mathrm{P}} < 1$. For the ranges $\tilde{\tau}_{ij,\mathrm{P}} \le 0$ and $\tilde{\tau}_{ij,\mathrm{P}} \ge 1$ the functional must equal $\tilde{\tau}_{ij,\mathrm{P}}$.

The MINMOD scheme adopted here combines the second order upwind scheme (SOU) with the central differencing scheme (CDS). In isolation, these schemes fail to satisfy the convection boundedness criterion, but not when they are combined as in Eq. (7), where $\tilde{\tau}_{ij,f}$ is equated as

$$\tilde{\tau}_{ij,f} = a + b\tilde{\tau}_{ij,\mathrm{P}} = \begin{cases} \dfrac{\tilde{\xi}_f}{\tilde{\xi}_{\mathrm{P}}}\tilde{\tau}_{ij,\mathrm{P}} & 0 < \tilde{\tau}_{ij,\mathrm{P}} < \tilde{\xi}_{\mathrm{P}} \quad (SOU) \\ \dfrac{\tilde{\xi}_f - \tilde{\xi}_{\mathrm{P}}}{1-\tilde{\xi}_{\mathrm{P}}} + \dfrac{1-\tilde{\xi}_{\mathrm{f}}}{1-\tilde{\xi}_{\mathrm{P}}}\tilde{\tau}_{ij,\mathrm{P}} & \tilde{\xi}_{\mathrm{P}} \le \tilde{\tau}_{ij,\mathrm{P}} < 1 \quad (CDS) \\ \tilde{\tau}_{ij,\mathrm{P}} & elsewhere \quad (UDS) \end{cases} \tag{7}$$

Using MINMOD, the convective flux in the stress equation is then given by

$$\frac{\lambda}{\rho}F_f\hat{\tau}_{ij,f}=\frac{\lambda}{\rho}F_f\hat{\tau}_{ij,f}=\frac{\lambda}{\rho}F_f\tau_{ij,\mathrm{P}}+\frac{\lambda}{\rho}F_f\left[a\left(\tau_{ij,\mathrm{D}}-\tau_{ij,\mathrm{U}}\right)+(b-1)\left(\tau_{ij,\mathrm{P}}-\tau_{ij,\mathrm{U}}\right)\right]_f \qquad (8)$$

where ^ symbolizes the MINMOD- interpolated stress at a cell face f.

3.3. Solution procedure and boundary conditions

The discretised equations for each variable are solved in a sequential manner and the revised version of the SIMPLEC algorithm of Van Doormal and Raithby [15], explained in [1], is used to apply the continuity equation for coupling pressure and velocity. Neither the algorithm nor the boundary conditions are affected by the use of the high-resolution scheme. To check for convergence, appropriate stopping criteria were applied and the implicit solution of the linear sets of equations at each time step was carried out with standard pre-conditioned conjugate gradient methods.

4. Flow problem

The plane flow past a circular cylinder in a channel was investigated and is represented schematically in Fig. 1. The flow has a plane of symmetry and only half of the domain needs to be calculated. The ratio of channel half-height h to cylinder radius R is equal to 2. The computational domain is $80R$ long, with $19R$ upstream and $59R$ downstream of the forward and rear stagnation points of the cylinder, respectively. The upstream and downstream lengths of the domain were sufficiently long to allow the full development of the flow well upstream of the cylinder and ensure a fully-developed outlet profile. All the calculations were carried out for Re=0. With U representing the bulk velocity in the channel, the relevant nondimensional Deborah number was defined as $De \equiv \lambda U/R$.

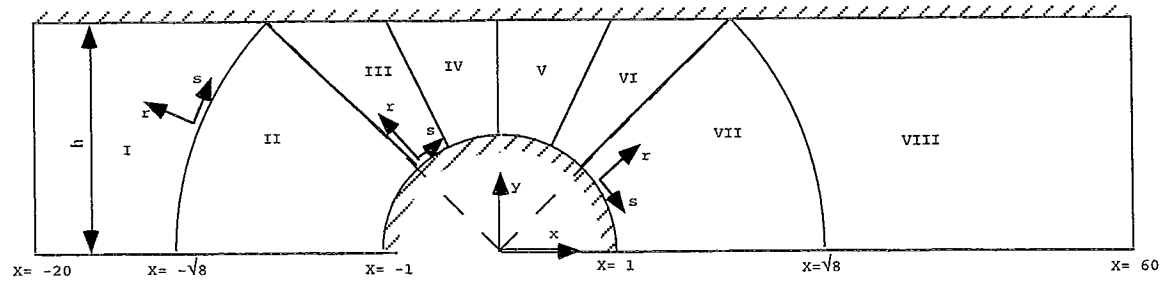

Figure 1- Schematic representation of the flow geometry and definition of the blocks used to generate the mesh (X=x/R, where R is cylinder radius). Flow is from left to right.

To generate the mesh the domain was divided into eight blocks as represented in Fig. 1. Within each block the cells were concentrated near the cylinder surface and the centreline in order to resolve adequately the stress boundary-layer. Five meshes with different degrees of refinement were used and their characteristics are presented in Table I. The meshes can be

grouped into two sets: (M45,M90) and (M60, M120), and within each set the refinement was consistently done, ie, between consecutive meshes the number of cells was doubled in each direction, with grid spacing being approximately halved following the procedure of Ferziger and Peric [16] to enable error estimation using Richardson's extrapolation to the limit.

Table 1- Main characteristics of the meshes NS x NR

Block	M45	M60	M75	M90	M120
I	38 x 36	50 x 48	62 x 60	75 x 72	100 x 96
II	38 x 45	50 x 60	62 x 75	75 x 90	100 x 120
III	19 x 45	25 x 60	31 x 75	38 x 90	50 x 120
IV	19 x 45	25 x 60	31 x 75	38 x 90	50 x 120
V	19 x 45	25 x 60	31 x 75	38 x 90	50 x 120
VI	19 x 45	25 x 60	31 x 75	38 x 90	50 x 120
VII	38 x 45	50 x 60	62 x 75	75 x 90	100 x 120
VIII	38 x 45	50 x 60	62 x 75	75 x 90	100 x 120
NCV	9918	17400	26970	39330	69600
$(\Delta r / R)_{\min}$ *	0.00646	0.00481	0.00383	0.00318	0.00238
$(\Delta s / R)_{\min}$ *	0.0207	0.0157	0.0127	0.0103	0.00785

NCV- Number of control volumes.
*Smallest cell all around the cylinder surface

5. Results and discussion

Results of the computations are presented in two ways: a scalar integral quantity representative of the flow, and detailed profiles of velocities and stress components in the vicinity of the cylinder. The integral quantity is the dimensionless drag force C_d resulting from the surface integration of the normalised stress τ' and pressure p' via

$$C_d \equiv \int_S (\tau' - p'\mathbf{I}) : \hat{\mathbf{i}} dS \tag{9}$$

where $\mathbf{I}$ is the identity tensor, $\hat{\mathbf{i}}$ is the unit vector in the x-direction and the superscript ' indicates that the stress tensor and pressure were normalised by $\eta U/R$.

Correct predictions of integral quantities are not synonymous of accurate predictions of the velocity and stress fields, because local variations of those quantities may compensate each other. Therefore, in order to ascertain the quality of the predictions velocity and stress profiles in the difficult stress boundary-layer and in the wake along the centreplane will also be shown. Both the drag force and these profiles will be compared with recent data from the literature [2].

Table 2 presents results of the drag force for all the cases that were simulated and includes extrapolated values of the drag force as well as data from the literature [2]. For the purpose of comparison upwind-based results are also included. The extrapolated data was based on the predictions from the M60 and M120 grids, using Richardson's technique, after determination of the order of convergence of the calculations with the different interpolation schemes. The order of convergence was obtained in two different, but related, procedures. In one of them, also used by [4], C_d was plotted as a function of the minimum grid spacing Δr and a fit of

$$C_d = C_{d_{extr}} + b(\Delta r)^n \tag{10}$$

gave the extrapolated C_d and the order of convergence n. A simpler trial-and-error method assumes that the extrapolated C_d from Richardson's technique represents the true value and plots the error $\left|C_d - C_{d_{true}}\right|$ as a function of Δr in log-log coordinates, the slope of which then gives the order of convergence, as shown in Fig. 2. To estimate the true C_d the nearer integer to the calculated order of convergence was used for the Richardson technique. Using both techniques, the following values for the order of convergence were determined: 1.1 for UDS and 1.9 for MINMOD at $De = 0.3$, and 0.9 for UDS and 1.8 for MINMOD at $De = 0.9$ (high elasticity case).

Table 2- Predicted drag coefficient on cylinder flow for the UCM fluid.

De	M45	M60	M75	M90	M120	Extrap.	[2] Mix1	[2] DEVSS
	with M30							
0	132.23	132.342			132.369		132.36	132.36
		126.799			127.141	127.483		
0.1		127.203			127.347	127.395	127.41	127.42
		117.077			117.485	117.893		
0.2		117.615			117.751	117.796	117.81	117.83
	107.806	108.043	108.178	108.264	108.385	108.727		
0.3	108.387	108.484	108.534	108.566	108.600	108.639	108.66	108.68
		101.134			101.300	101.466		
0.4		101.265			101.344	101.370	101.41	101.43
		96.390			96.275	96.160		
0.5		95.984			96.030	96.045	96.08	96.11
		93.467			92.970	92.473		
0.6		92.302			92.306	92.307	92.33	92.37
		91.973			90.995	90.017		
0.7		89.857			89.799	89.780	89.79	89.84
		91.578			90.039	88.500		
0.8		88.359			88.207	88.156		88.18
	93.113	92.029	91.221	90.581	89.856	87.683		
0.9	87.850	87.585	87.452	87.373	87.277	87.174		
		93.063			90.268	87.473		
1.0		87.272			86.750	86.576		
		94.630			90.995	87.360		
1.1		87.355			diverges			
1.2		96.828			diverges			
1.3		98.942						
1.4		102.060						
1.5		104.575						

First result with UDS and second with MINMOD (when available)

The most recent results for UCM flow in this geometry are those of [2] using the MIX1 and DEVSS finite-element formulations. Fan et al [2] claim that MIX1 is the best formulation of the two, hence the corresponding values are compared with our predictions in mesh M120 in Fig. 3. For $De \leq 0.5$ there is clearly a good agreement between all predictions, although the UDS values show its lower accuracy. All the extrapolated values differ by less than 0.1% from the MIX1 results, which were also very close to the DEVSS predictions. The differences are of the order of 0.06% to 0.08% for UDS, and between 0.01% and 0.04% for MINMOD. These characteristics are confirmed in the comparisons involving the M120 grid predictions. The

figure also highlights the benefits of the high-resolution scheme: the differences relative to MIX1 rise above 0.2% for UDS, but stay below 0.05-0.06% for MINMOD.

In the low Deborah number range ($De < 0.5$) no major differences were expected between the various sets of predictions, since it is known from the literature that the various formulations are basically in agreement. However, it is important to emphasize that our predictions with the HR-scheme and Richardson extrapolation give consistently lower values than the MIX1 results of Fan et al. These authors claimed their predictions of C_d to be the most accurate in the literature for this benchmark problem on the basis that most other results show substantially higher values of C_d and, they said, that is consistent with a deterioration of accuracy. The present predictions give support to that assertion in an independent way and suggest that the true value of C_d may be even lower.

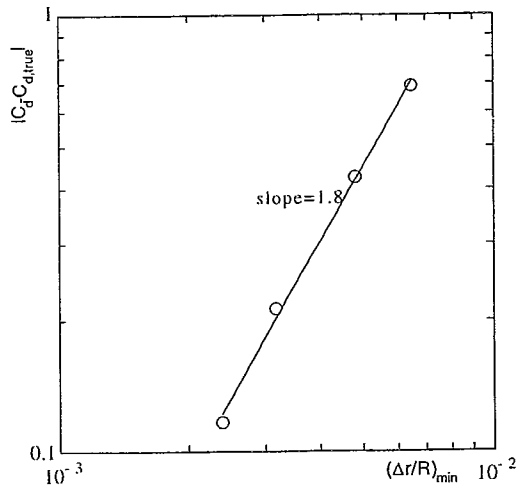

Figure 2- Convergence of C_d with mesh refinement (De=0.9, UCM, MINMOD).

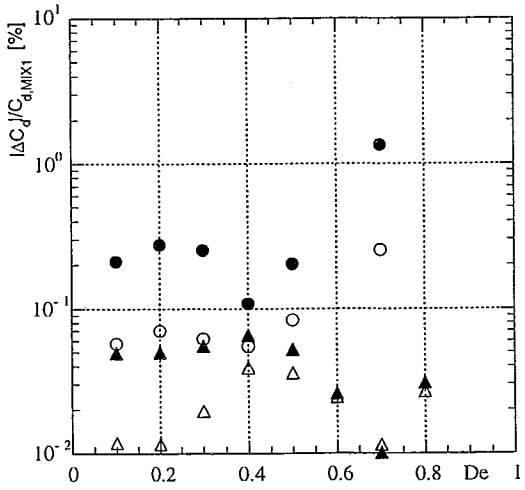

Figure 3- Relative difference between the present C_d's and those from [2] with MIX1 formulation (O UDS; Δ MINMOD. Open symbols: extrapolated; Closed symbol: M120)

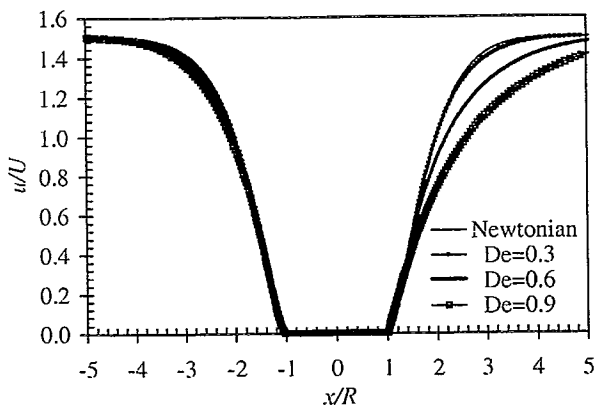

Figure 4- Profile of the axial velocity component along the centreline (MINMOD, mesh M120).

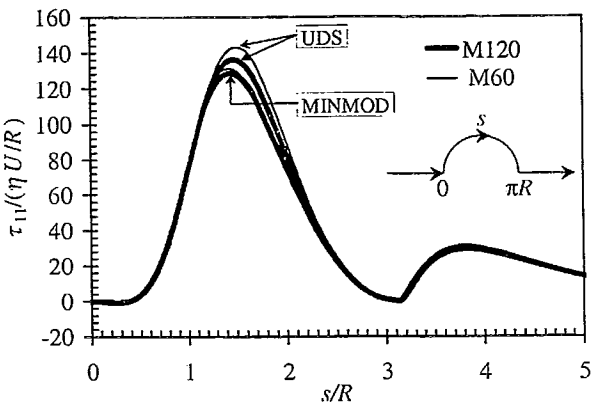

Figure 5- Profile of the axial normal stress component along the cylinder surface and the centreline for De=0.6.

For higher Deborah numbers ($De > 0.5$) the predictions of UDS deteriorate considerably: at De=0.7 the differences relative to MIX1 are of 0.25% and 1.3% for the extrapolated and M120 values, whereas for MINMOD the differences still remain at about 0.04%.

Profiles of the normalised axial velocity along the centreline and cylinder surface for Newtonian and UCM fluids are compared in Fig. 4 for different *De* numbers. The Newtonian flow is perfectly symmetric, but elasticity elongates the recovery zone. The corresponding profiles of the normalised axial normal stress at $De= 0.6$, calculated with UDS and MINMOD in meshes M60 and M120, are plotted in Fig. 5 and show two maxima. The first maximum, located in the narrowest part of the channel, is lower for MINMOD and the values from both meshes are very close to each other, whereas with UDS the stresses are higher and the differences between the two meshes are larger, thus showing the better convergence of the high-resolution scheme. The second maximum occurs at the wake, downstream of the rear stagnation point, and there one can not distinguish differences between both MINMOD solutions and the M60 UDS curve is slightly below all the others.

Acknowledgements

PJO acknowledges support by Centro de Materiais Têxteis e Papeleiros, of UBI and MAA whishes to thank his Dep. de Eng. Química at FEUP for a temporary leave of absence.

References

[1] P. J. Oliveira, F. T. Pinho, G. A. Pinto, *J. Non-Newt. Fluid Mech.*, 79 (1998) 1-43.

[2] Y. Fan, R. I. Tanner, N. Phan-Thien, *J. Non-Newt Fluid Mech.*, 84 (1999) 233-256.

[3] R. A. Brown, G. H. McKinley, *J. Non-Newt. Fluid Mech.* 52 (1994) 407-413

[4] A. W. Liu, D. E. Bornside, R. C. Armstrong, R. A. Brown, *J. Non- Newt. Fluid Mech.* 77 (1998) 153-190.

[5] J. Sun, M. D. Smith, R. C. Armstrong, R. A. Brown, *J. Non-Newt Fluid Mech*, 86 (1999) 281-307.

[6] X. Huang, N. Phan-Thien, R. I. Tanner, *J. Non-Newt. Fluid Mech.* 64 (1996) 71-92.

[7] S.-C. Xue, N. Phan- Thien, R. I. Tanner, *J. Non-Newt Fluid Mech*, 74 (1998) 195-245.

[8] H.- S. Dou and N. Phan-Thien, *J. Non-Newt. Fluid Mech.* 87 (1999) 47-73

[9] P. J. Oliveira, F. T. Pinho, *Numerical Heat Transfer.Part B*, 35 (1999) 295-315.

[10] P. J. Oliveira, F. T. Pinho, *J. Non-Newt. Fluid Mech.*, 88 (1999) 63-88.

[11] S. G. Rubin, P. K. Khosla, *Comp. and Fluids*, 2 (1974) 207-209

[12] C. M. Rhie, W. L. Chow, *AIAAJ*, 21 (1983) 1525-1532.

[13] M. S. Darwish, F. Moukalled, *Num. Heat Transfer, Part B*, 26 (1994) 79-96.

[14] P. H. Gaskell, A. K. C. Lau, *Int. J. Numer. Meth. Fluids*, 8 (1988) 617-641.

[15] J. P. Van Doormal, G. D. Raithby, *Num. Heat Transfer*, 7 (1984) 147-163.

[16] J. H. Ferziger, M. Peric, *Int. J. Num. Meth. Fluids*, 23 (1996) 1263-1274.